Mixing induced by Rayleigh–Taylor instability in a vortex

Article *in* Physics of Fluids · February 2005

Impact Factor: 2.03 · DOI: 10.1063/1.1852580

3 authors:

Laure Coquart
French National Centre for Scientific Research
9 PUBLICATIONS **211** CITATIONS
SEE PROFILE

Denis Sipp
The French Aeropace Lab ONERA
99 PUBLICATIONS **1,337** CITATIONS
SEE PROFILE

Laurent Jacquin
The French Aeropace Lab - ONERA, Ecole Pol…
123 PUBLICATIONS **2,035** CITATIONS
SEE PROFILE

Mixing induced by Rayleigh–Taylor instability in a vortex

Laure Coquart,[a] Denis Sipp, and Laurent Jacquin
ONERA, 8 rue des Vertugadins, 92190 Meudon, France

(Received 28 October 2004; accepted 7 December 2004; published online 19 January 2005)

The direct numerical simulation (DNS) of a two-dimensional Lamb–Oseen vortex with a heavy internal core has been performed. Linear stability theory predicts the existence of Rayleigh–Taylor (RT) instabilities due to the destabilizing effect of the centrifugal force on the radial flow nonhomogeneities. The DNS first exhibits wavy azimuthal perturbations which are nonlinearly distorted into bubble-like patterns, characteristic of the standard development of the RT instabilities, i.e., instabilities obtained in a planar nonhomogeneous flow in the presence of gravity. Nevertheless, important differences may be observed in the late stage development of the instability: contrary to the standard case, the bubbles are then stretched in the azimuthal direction leading to a strong radial filamentation of the flow. © *2005 American Institute of Physics*. [DOI: 10.1063/1.1852580]

Stabilizing mechanisms associated to rotation usually make a vortex very resistant to radial momentum diffusion.[1,2] The present Letter is considering possible density variation effects to achieve this goal. If density effects were significant, vortex control by means of injection of heated or cooled air could be considered, for example, in the application of aircraft wakes.[3] The goal of this Letter is, precisely, to evaluate the potential of such density effects on the dynamics of vortex cores.

The linear stability of a compressible two-dimensional (2D) Lamb–Oseen vortex with a heavy core predicts the existence of 2D temporally oscillating unstable modes.[4] These unstable modes are of the Rayleigh–Taylor (RT) type. As a matter of fact, heavy fluid inside light fluid in a vortex core is equivalent to light fluid below heavy fluid in the presence of gravity. The gravity force is replaced here by the centrifugal force. In both cases, the unstable situation corresponds to the force (gravity or centrifugal) directed towards the light fluid. In this Letter, we study the linear and nonlinear development of these instabilities thanks to a 2D direct numerical simulation (DNS). The main objective of this Letter is to characterize possible differences that may exist in the development of RT instabilities between the standard case with the gravity force and the present situation with the centrifugal force.

Let L_{ref}, u_{ref}, ρ_{ref} and T_{ref} be the reference length, velocity, density, and temperature scales of the problem. These reference scales will be precised below. The compressible Navier–Stokes equations read in nondimensional form

$$\partial_t \rho + \partial_i(\rho u_i) = 0, \tag{1}$$

$$\partial_t(\rho u_i) + \partial_j(\rho u_i u_j) = -\partial_i p + \frac{\partial_j \tau_{ij}}{\mathcal{R}}, \tag{2}$$

$$\partial_t E + \partial_i[(E+p)u_i] = \frac{\partial_i(\tau_{ij}u_j)}{\mathcal{R}} + \frac{\partial_i\partial_i T}{(\gamma-1)\mathcal{P}\mathcal{M}^2\mathcal{R}}, \tag{3}$$

where u_i, ρ, T, p are the velocity, density, temperature, and pressure of the fluid, $\tau_{ij}=\partial_j u_i+\partial_i u_j-2\delta_{ij}\partial_k u_k/3$ is the viscous stress tensor and $E=p/(\gamma-1)+\rho u_i u_i/2$ is the total energy. The flow is supposed to behave like a perfect gas: $\gamma\mathcal{M}^2 p=\rho T$. Several nondimensional parameters appear: the Reynolds number $\mathcal{R}=u_{ref}L_{ref}\rho_{ref}/\mu$ where μ is the viscosity, the Mach number $\mathcal{M}=u_{ref}/(\gamma \mathrm{R} T_{ref})^{1/2}$ where R is the constant of perfect gas, the specific heat ratio γ, the Prandtl number $\mathcal{P}=\mu c_p/k$, where c_p and k designate the specific heat at constant pressure and the thermal conductivity. The simulation is performed at a low Mach number so that the static temperature variations are small. This allows us to make the assumption of constant viscosity, constant thermal conductivity and constant specific heats.

These equations are solved on a Cartesian grid mesh. Time integration of the equations is decoupled from spatial discretization and is perfomed by a third order Runge–Kutta scheme with the numerical coefficients of Lowery and Reynolds.[5] The convective terms are discretized with a sixth-order compact finite differences scheme.[6] To minimize the aliasing errors, the nonlinear terms are written in the skew symmetric form.[7] Diffusive terms are evaluated with a sixth-order accurate scheme, except the diagonal terms that are discretized by using a scheme introducing enough numerical dissipation to avoid oscillations.[8] Nonreflecting boundary conditions are prescribed at the lateral boundaries.[9]

The flow field is initialized by the superposition of a basic flow and a perturbation. The basic flow is an axisymmetric vortex with radial variations of the density profile. Hence, if u_r and u_θ designate the radial and azimuthal velocity components in cylindrical (r,θ) coordinates, the basic flow reads: $[u_r,u_\theta,p,\rho]=[0,V(r),P(r),R(r)]$. The velocity field $V(r)$ is chosen to be the azimuthal velocity profile of the Lamb–Oseen vortex:

[a]Telephone: 33 (0)1 46 23 51 64. Fax: 33 (0)1 46 23 51 58. Electronic mail: Laure.Coquart@onera.fr

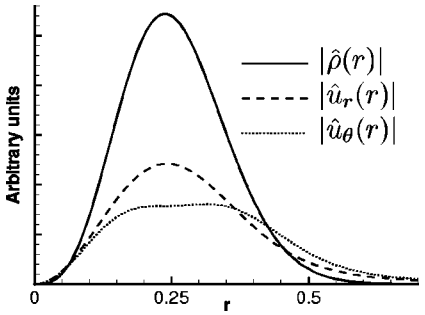

FIG. 1. Modulus of the eigenfunctions $\hat{\rho}(r)$, $\hat{u}_r(r)$, and $\hat{u}_\theta(r)$ associated to the eigenmode characterized by $(\sigma=0.20, \omega_r=2.82)$, $m=3$, $b=0.3$, $s=0.2$, $\mathcal{M}=0.1$, $\gamma=1.4$, $\mathcal{R}=10\,000$, and $\mathcal{P}=0.7$.

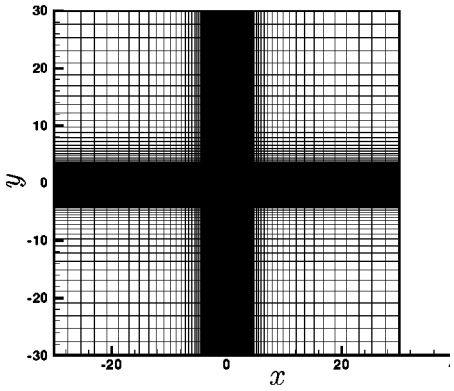

FIG. 2. Computational domain and grid mesh.

$$V=\frac{1-\exp(-r^2)}{r}. \tag{4}$$

The reference length and velocity scales L_{ref} and u_{ref} therefore designate the characteristic radius and velocity of the Lamb–Oseen vortex. In addition, for the definition of the Mach number $\mathcal{M}$, we choose the static temperature of the fluid at infinity as the reference temperature scale T_{ref}. The density distribution $R(r)$ is prescribed as

$$R=1+s\exp(-r^2/b^2), \tag{5}$$

where s and b designate the amplitude and width of the heavy internal core. The reference density scale ρ_{ref} is therefore equal to the density at infinity. The pressure $P(r)$ is obtained by integrating the radial momentum equation:

$$P=\frac{1}{\gamma\mathcal{M}^2}-\int_r^\infty \frac{RV^2}{r}dr. \tag{6}$$

This flow field is a steady solution of the Euler equations while it slightly diffuses in time in the presence of viscosity.

The perturbation is constituted of a small amplitude eigenmode of the linearized Navier–Stokes equations around the basic flow (4)–(6). This eigenmode is calculated thanks to a matrix eigenvalue–eigenvector method based on a spectral Chebyshev collocation. If Re designates the real part of a complex, the unstable eigenmode may be written as

$$[u_r', u_\theta', p', \rho', T'] = \mathrm{Re}(A[\hat{u}_r(r), \hat{u}_\theta(r), \hat{p}(r), \hat{\rho}(r), \hat{T}(r)]e^{i(m\theta-\omega t)}), \tag{7}$$

where m is the azimuthal wavenumber, ω is the complex frequency $\omega=\omega_r+i\sigma$, and A is the amplitude of the eigenmode. A Lamb–Oseen vortex with a heavy internal core ($s>0$) is generically unstable to RT instabilities. The involved physical mechanims are incompressible and inviscid. In the following, we therefore choose a low value for the Mach number and a high value for the Reynolds number. More precisely, the case investigated in this Letter corresponds to $b=0.3$, $s=0.2$, $\mathcal{M}=0.1$, $\gamma=1.4$, $\mathcal{R}=10\,000$, and $\mathcal{P}=0.7$. It appears that the most unstable eigenmode in this situation corresponds to an $m=3$ eigenmode with $(\sigma=0.20, \omega_r=2.82)$. The associated eigenfunctions $\hat{\rho}(r)$, $\hat{u}_r(r)$ and $\hat{u}_\theta(r)$ are represented in Fig. 1. For the initialization of the simulation, the amplitude A of the eigenmode in Eq. (7) is adjusted so as to have $\max\{\rho'\}=0.02\max\{R\}$.

The computational domain is represented in Fig. 2. Its dimensions are: $-30\leqslant x, y\leqslant 30$. The grid is uniform in the domain $-3\leqslant x, y\leqslant 3$ and is stretched using a monotonic tanh law up to the boundaries. The mesh has $N_x=681$ and $N_y=681$ points. The density peak is described with 30 points and the core of the vortex with 100 points.[10] The time step is $\Delta t=5\cdot 10^{-4}$, which corresponds to CFL=0.55.

At each time step, we evaluate the mean density and azimuthal velocity profiles by averaging over θ. For instance,

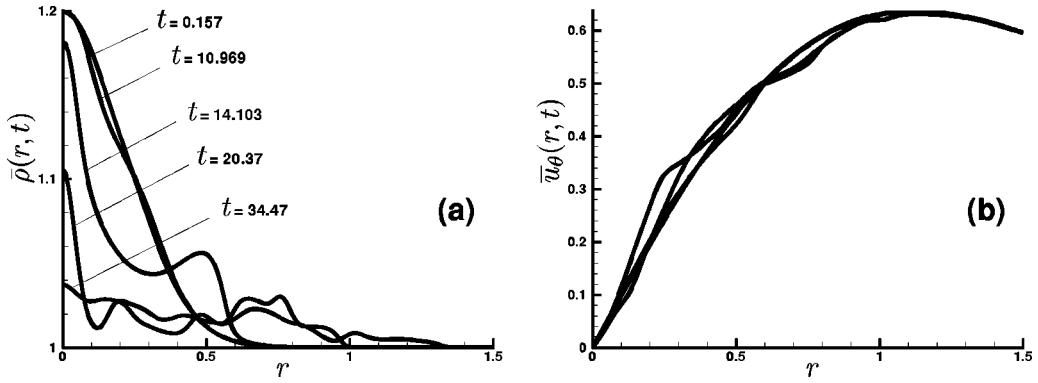

FIG. 3. Evolution of (a) $\overline{\rho}(r,t)$ and (b) $\overline{u_\theta}(r,t)$ as a function of the radius r for $t=0.157$; $t=10.969$; $t=14.103$; $t=20.37$; $t=34.47$.

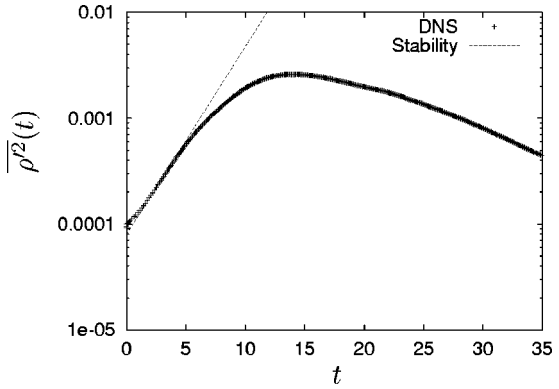

FIG. 4. Amplitude of the perturbation $\overline{\rho'^2}(t)$ as a function of time t.

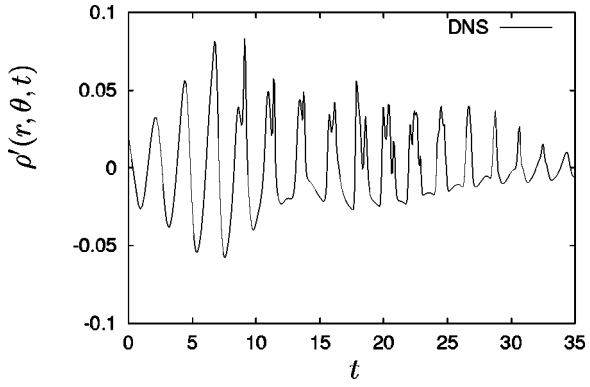

FIG. 5. Density fluctuations $\rho'(r,\theta,t)$ at $(x=0.289, y=0)$ as a function of time t.

$\overline{\rho}(r,t)=(1/2\pi)\int_0^{2\pi}\rho(r,\theta,t)d\theta$. Figures 3(a) and 3(b) represent these two quantities, i.e., $\overline{\rho}(r,t)$ and $\overline{u_\theta}(r,t)$ as functions of the radius r at various times t. We can see that the Gaussian density peak collapses as time evolves while the azimuthal velocity field of the vortex remains nearly unchanged. Hence, as the instability develops, the nonlinear interactions destroy the density peak of the mean flow, which renders the flow stable to RT instabilities.

The density fluctuations are then evaluated following $\rho'(r,\theta,t)=\rho(r,\theta,t)-\overline{\rho}(r,t)$. The overall amplitude of the perturbation may be obtained from an integral over the calculation box of the square of the density fluctuations: $\overline{\rho'^2}(t)=\int_0^\infty\int_0^{2\pi}[\rho'(r,\theta,t)]^2 r dr d\theta$. Figure 4 shows this quantity as a function of time t. Its growth rate may be compared to the amplification rate obtained from the linear stability analysis. Agreement is very good in the linear phase, i.e., up to $t\simeq 5$. Then, the mean amplitude of the perturbation saturates at $t\simeq 10$ before decreasing slowly with time. For $t>20$, as shown before, the density peak of the mean flow collapses as time evolves. Hence, the driving force of the instability vanishes which induces the loss of the perturbation source. The density fluctuations therefore die out and the vortex flow becomes laminar.

Figure 5 shows the density fluctuations $\rho'(r,\theta,t)$ obtained at $(x=0.289, y=0)$ as a function of time t. In the linear regime, i.e., for $t\leqslant 5$, the signal exhibits a time period equal to $\Delta t=2.2$. This value is compatible with the linear stability

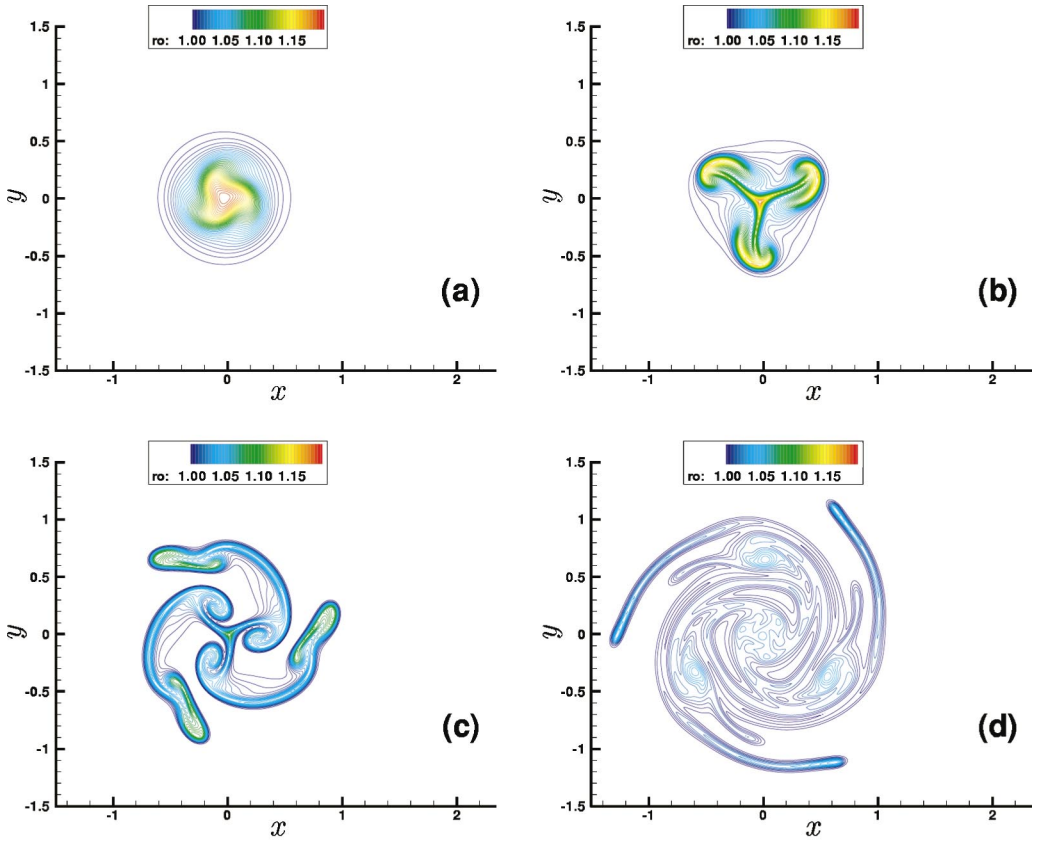

FIG. 6. (Color). Density $\rho(r,\theta,t)$ at different times: (a) $t=0.157$; (b) $t=10.969$; (c) $t=20.37$; (d) $t=34.47$.

analysis which predicts a time period equal to $\Delta t = 2\pi/\omega_r = 2.2$. In the nonlinear regime, the signal becomes more abrupt and decreases in amplitude.

Figure 6 presents density isovalues at four distinct times. In Fig. 6(a), the RT instability starts growing linearly. In Fig. 6(b), we enter the nonlinear regime: the flow exhibits the mushroom-like patterns characteristic of the nonlinear development of the RT instability.[11] In Fig. 6(c), which corresponds to the late stage development of the instability, we observe nonstandard features. Usually, i.e., in the case of standard nonhomogeneous flows with gravity, the RT mushroom-like patterns just continue to spread while new secondary instabilities complexify the overall flow structure. In the case of a vortex with a heavy internal core, the mushroom-like patterns are strongly stretched in the azimuthal direction and subject to filamentation.These differences are due to the azimuthal velocity of the vortex which is not present in the standard case. Comparing Fig. 6(b) to Fig. 6(c), it can also be observed that the intensity of the perturbations decreases with time. As shown in Fig. 6(d), a complex lamellar structure is finally obtained in the vortex core.

To conclude, we have performed a 2D DNS of the RT instability which develops in a vortex with a heavy internal core. The results show that after a phase of linear growth, the amplitude of the perturbation saturates and finally decreases. The nonlinear interactions destroy the density peak of the mean flow, which is precisely the driving force of the instability. Hence, the mean flow becomes stable to RT instabilities, which leads to the loss of the perturbation source. Also, in the late stage development of the nonlinear regime, we have shown that the azimuthal velocity of the vortex violently stretches the perturbations in the azimuthal direction leading to a strong radial filamentation of the flow. Hence, the nonlinear evolution of the RT instabilities obtained here is radically different from the standard case of RT instabilities developing in a planar nonhomogeneous flow in the presence of gravity. This shows that differential rotation may deeply affect the development of RT instabilities. Considering practical applications, the potential of density effects on the momentum diffusion of a vortex is poor. But, the mechanisms described above also show that one obtains very efficient mixing which remains localized within the vortex core. These properties may have interesting applications in the field of mixing and combustion.

[1] O. Zeman, "The persistence of trailing vortices: A modeling study," Phys. Fluids **7**, 135 (1995).
[2] L. Jacquin and C. Pantano, "On the persistence of trailing vortices," J. Fluid Mech. **471**, 159 (2002).
[3] P. R. Spalart, "Airplane trailing vortices," Annu. Rev. Fluid Mech. **30**, 107 (1998).
[4] D. Sipp, D. Fabre, S. Michelin, and L. Jacquin, "Stability of a vortex with a heavy core," J. Fluid Mech. (to be published).
[5] P. S. Lowery and W. C. Reynolds, "Numerical simulation of spatially developing forced plane mixing layer," Stanford University, Report No. TF-26, 1986.
[6] S. Lele, "Compact finite differences schemes with spectral resolution," J. Comput. Phys. **103**, 16 (1992).
[7] G. A. Blaisdell, E. T. Spyropoulos, and J. H. Qin, "The effect of the formulation of nonlinear terms on aliasing errors in spectral methods," Appl. Numer. Math. **21**, 207 (1996).
[8] C. F. Gago, S. Brunet, and F. Garnier, "Numerical investigation of turbulent mixing in a jet/wake vortex interaction," AIAA J. **40**, 276 (2002).
[9] K. W. Thompson, "Time dependent boundary conditions for hyperbolic systems," J. Comput. Phys. **68**, 1 (1987).
[10] M. Sreedhar and S. Ragab, "Large eddy simulation of longitudinal stationary vortices," Phys. Fluids **6**, 2501 (1994).
[11] T. T. Clark, "A numerical study of the statistics of a two-dimensional Rayleigh–Taylor mixing layer," Phys. Fluids **15**, 2413 (2003).